Chapter 5
ALTERNATE FATIGUE TEST AND TESTING GEOMETRY

5.1 Prologue

The parallel plate cylindrical geometry is the most common and conventional DSR geometry with an 8 mm diameter and 2 mm height. The hyperbolic geometry, on the other hand, is also a PP08 (parallel plate with 8 mm diameter) geometry but with a sample height of 3 mm and a predetermined point of failure at the center of the specimen. The circular necking extending from the ends to the center allows a gradual decrease in the diameter from 8 mm to 6 mm. The unfavorable stress concentrations at both ends are minimized by raising a small platform of 0.3 mm at both ends. One of the most important advantages of using hyperbolic geometry is that it can be fabricated in the conventional PP setup, which comes with every DSR. It does not require a separate setup as in the case of a torsion cylinder or vane shear geometry. Also, the pre-determined point of failure ensures true cohesion failure within the specimen. The elevation view for both geometries and the testing pictures are shown in Figure 5.1 to highlight the fundamental difference between them.

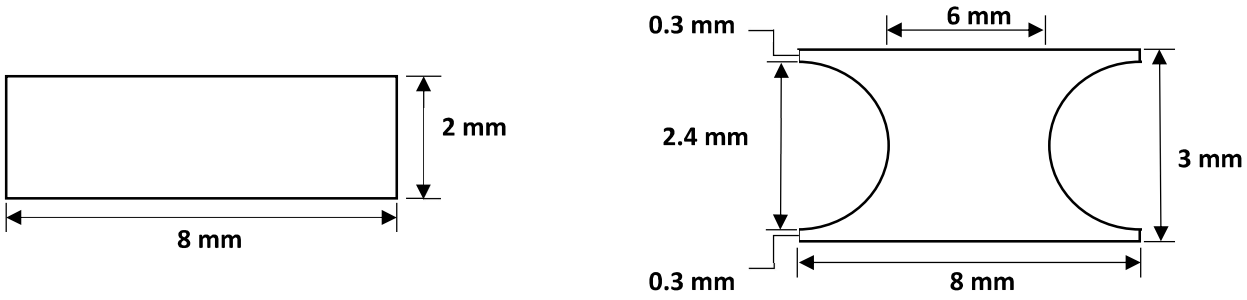

(a) (b)

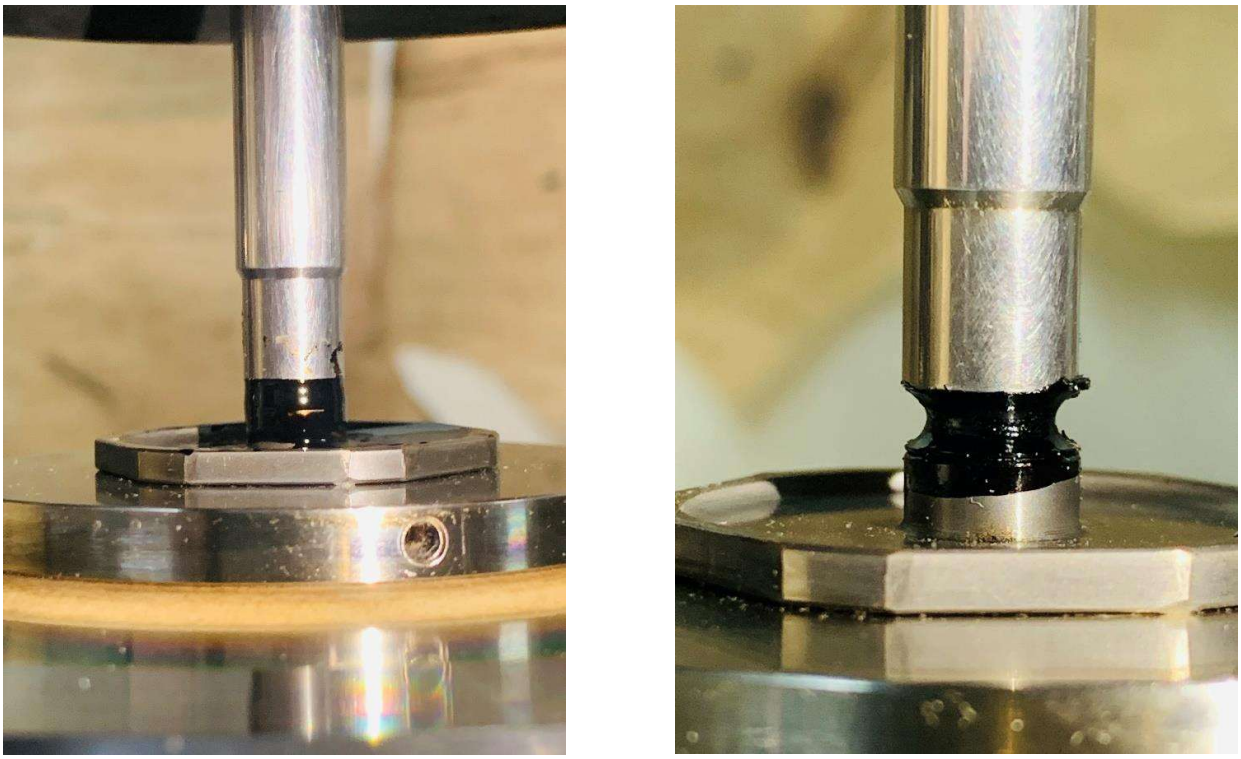

(c) **(d)**

Figure 5.1 Elevation view and testing picture of (a), (c) cylindrical geometry and (b), (d) hyperbolic geometry

The DSR measures/controls only two properties in the form of torque and angular rotation directly based on all other calculations within the DSR software [41,157]. The shear stress and shear strains are calculated using these measurements coupled with the radius and height of the sample as follows:

$$\tau = \frac{2T}{\pi r^3} \tag{5.1}$$

$$\gamma = \frac{r.\theta}{h} \tag{5.2}$$

Dividing equation 5.1 by equation 5.2 yields the following expression for complex shear modulus (|G*|):

$$|G^*| = \frac{2Th}{\pi r^4 \theta} \tag{5.3}$$

Where G^* is the complex shear modulus ($N/mm^{2)}$), τ is the shear stress ($N/mm^{2)}$), γ is the shear strain, T is the torque (N.mm), r is the radius of the sample (mm), θ is the deflection angle (radians) and h is the plate gap (mm).

The DSR calculates the properties of the sample based on the aforementioned equations. It has attachments for only two specimen diameters, i.e., 25 mm and 8 mm. All the calculations are based on those only, but the hyperbolic sample's diameter gradually decreases from 8 mm to 6 mm. In this study, it is assumed that the contributing diameter is 6 mm to account for the critical situations. Hospodka et al. [17] in his study, also reported the same observation as the stress in the sample was found to be highest at the centre where the sample diameter is 6 mm. Due to this, the rheological parameters like shear stress, shear strain, and complex modulus calculated from these equations cannot be directly used and require a correction factor through which the true parameters corresponding to a hyperbolic geometry with a diameter of 6 mm and specimen height of 3 mm can be obtained [17].

The calculation for the correction factor is described in the upcoming section:

5.2 Correction Factors

5.2.1 Correction Factor for Shear Stress

The ratio of the shear stress in hyperbolic and cylindrical geometry can be obtained from Equation (5.1) as:

$$\frac{\tau_H}{\tau_C} = \frac{{r_C}^3}{{r_H}^3} \tag{5.4}$$

or

$$\frac{\tau_H}{\tau_C} = \left(\frac{r_C}{r_H}\right)^3 \tag{5.5}$$

The radius of the cylindrical specimen (r_C) is 4 mm, whereas that of the hyperbolic specimen (r_H) is 3 mm. Hence,

$$\tau_H = 2.37 * \tau_C \tag{5.6}$$

Hence, the actual shear stress in the hyperbolic specimen can be calculated by multiplying a correction factor of 2.37 to the obtained value.

5.2.2 Correction Factor for Shear Strain

The ratio of the shear strain in hyperbolic and cylindrical geometry can be obtained from Equation (5.2) as:

$$\frac{\gamma_H}{\gamma_C} = \frac{r_H}{r_C} \tag{5.7}$$

or

$$\frac{\gamma_H}{\gamma_C} = \frac{3}{4} \tag{5.8}$$

Hence,

$$\gamma_H = 0.75 * \gamma_C \tag{5.9}$$

Therefore, the actual shear strain in the hyperbolic specimen is 75% of that applied by the DSR.

5.2.3 Correction Factor for Complex Modulus

The ratio of complex shear modulus in hyperbolic and cylindrical geometry can be obtained from equation 5.3 as:

$$\frac{|G^*{}_H|}{|G^*{}_C|} = \frac{{r_C}^4}{{r_H}^4} \tag{5.10}$$

or

$$\frac{|G^*_H|}{|G^*_C|} = \left(\frac{r_C}{r_H}\right)^4 \tag{5.11}$$

Substituting the values r_C and r_H as 4 and 3, respectively, in the above equation yields the following expression:

$$|G^*_H| = 3.16 * |G^*_C| \tag{5.12}$$

This implies that the actual stiffness of the samples is 3.16 times that reported by the DSR.

It is to be noted all the calculations and analyses in this study are done by applying the aforementioned correction factors to the raw values obtained from the DSR. The values of the correction factors are considerably higher, which shows that the results can be erroneous to a very high degree if the correction factors are not applied while using the new geometry. It is to ne noted that the aforementioned correction factors are the approximate values derived from the fundamental mathematical equations, however, the exact values may vary depending on various factors which can be explored in the future studies.

5.3 Fabrication of Hyperbolic Geometry Mold

The hyperbolic molds are prepared following a simple fabrication procedure, as shown in Figure 5.2. It involves combining a TFC silicon rubber type 12 base and the catalyst in a weight ratio of 1:1. Both components were shaken, and equal proportions from each component were separated and mixed carefully with the help of a mixing tool such that there were no entrapped air bubbles. The prepared homogenous mixture was then poured into the metal mold using a thin pouring stream. The mixture was allowed to cool for 60 minutes and removed from the metal mold to obtain the required hyperbolic mold to be used in DSR to prepare the hyperbolic specimens.

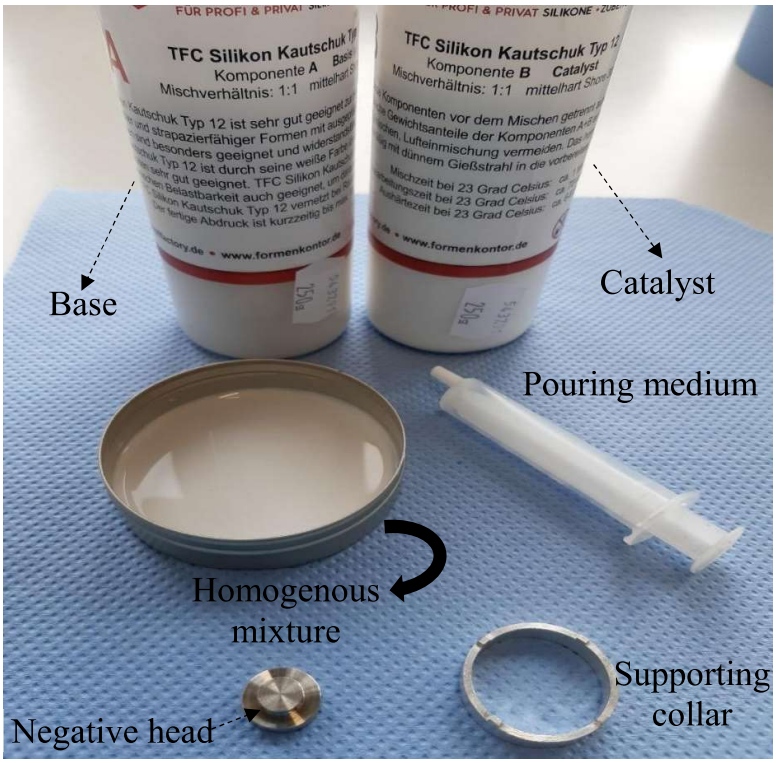
TFC Silikon Kautschuk
Komponente A
Mischverhältnis: 1:1
TFC Silikon Kautschuk Typ 12
Komponente B Catalyst
Mischverhältnis: 1:1
Base
Catalyst
Pouring medium
Homogenous mixture
Supporting collar
Negative head

(a)

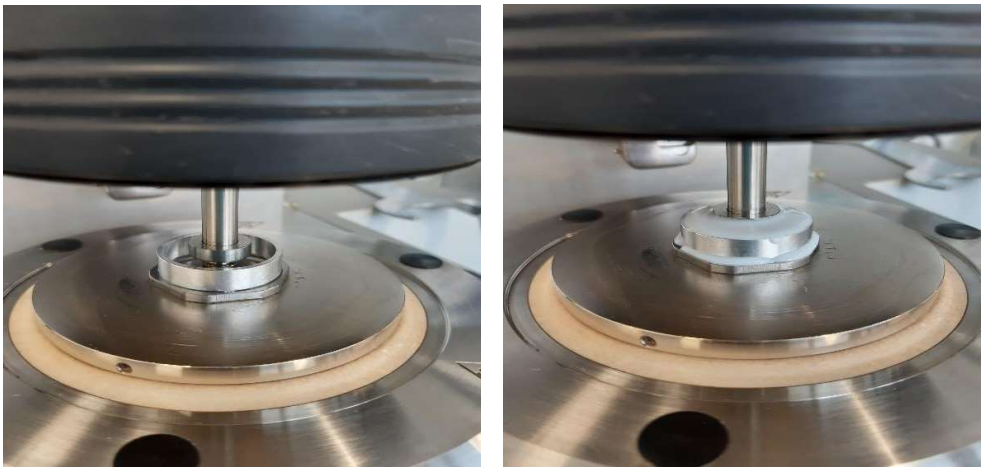

(b)

(c)

Figure 5.2 Hyperbolic mold fabrication procedure (a) materials used (b) cooling of mold (c) prepared mold

5.4 Hyperbolic Geometry Fabrication

The hyperbolic specimen was prepared in the DSR following a set of operations, as shown in Figure 5.3. The procedure consists of placing the hyperbolic mold on the lower plate of the DSR and confining it with the rubber band to prevent the distortion of shape. The molten asphalt sample was poured into the mold, and the spindle was lowered such that the height of the specimen became 3 mm. The temperature of the DSR was lowered to 15^{o}C, and the assembly was left undisturbed for the equilibrium time of 10 minutes at the same temperature. The rubber band and the mold were removed, and the required hyperbolic specimen was obtained for testing. Unlike cylindrical specimens, it does not require any trimming operation; due to this, the trimming-related errors are minimized in the hyperbolic geometry.

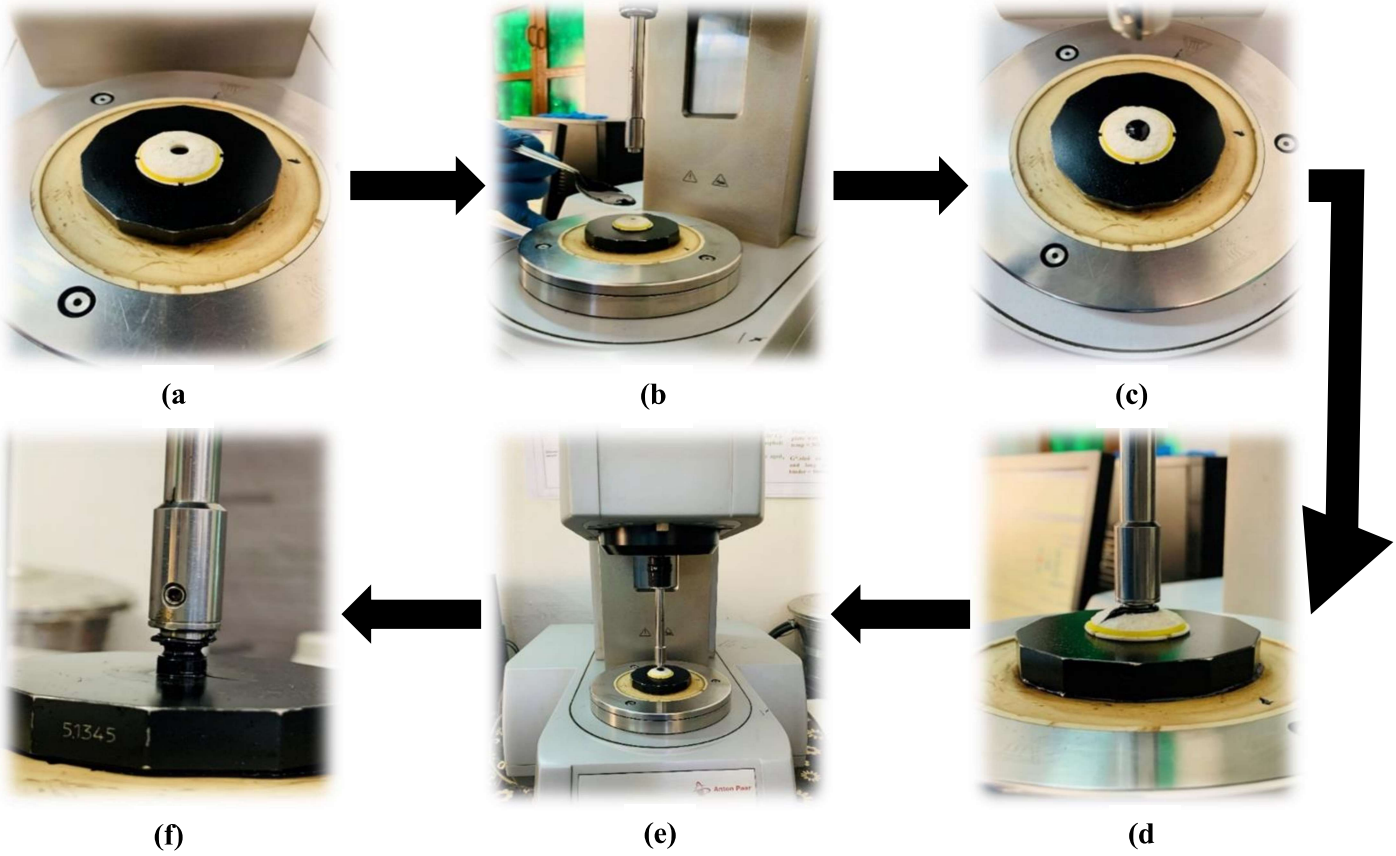

Figure 5.3 Preparation of hyperbolic specimen in sequential images

5.5 Suitability of LAS Test as an Alternative to TS Test

The first objective of this chapter is to assess the suitability of the LAS test as a surrogate for the conventional TS test for the fatigue analysis of asphalt binders and asphalt mastics. To accomplish this, fatigue testing was done on both the geometries using TS and LAS tests. The Dissipated Energy Ratio (DER) approach has been employed to determine the fatigue life of the samples via the TS test in this study. It was introduced by Pronk and Hopman in 1991 [312,313] to define the fatigue failure point and is one of the most popular approaches. The DER approach has been successfully applied by several other studies as well [161,313]. The expression for dissipated energy at each loading cycle is:

$$W_i = \pi \cdot \sigma_i \cdot \gamma_i \cdot \sin(\delta_i) \quad (5.13)$$

Where,

W_i, σ_i, γ_i, and δ_i are the dissipated energy, stress level, strain level, and phase angle in cycle i. The DER is defined as the ratio of cumulative dissipated energy till load cycle n and the dissipated energy in load cycle n, as shown in the equation below:

$$DER = \frac{\sum_{i=1}^{n} W_i}{W_n} \quad (5.14)$$

The variation of DER is linear, with the loading cycles signifying the undamaged sample. However, the DER deviates from the linear trend after the subsequent loading cycles, representing the onset of fatigue damage. Bonnetti [149] proposed a parameter known as N_{p20} that describes the loading cycles corresponding to the 20% deviation of DER from the undamaged linear line. A similar fatigue failure criterion has been used in this study for the TS test. The determination of the fatigue life of the samples by LAS test was done using both DE and PSE approaches; their detailed derivation is already discussed in sections 2.4.4.3.1 and 2.4.4.3.2. In addition, the Superpave fatigue parameter, i.e., |G*|.sinδ was also calculated through the LAS test. The strain level of 5%, which corresponds to the binder strain in the weak pavement [314,315] was chosen to compare the fatigue results; the detailed reason for the same is explained in Chapter 6 Section 6.5.2. The different methods used for the analysis of test results are described as follows:

5.5.1 Correlation Analysis

The correlation analysis was used to find the interrelation between the fatigue life (no. of cycles to failure, N_f) obtained from the TS test (N_f (TS)) and the remaining three variables, i.e., N_f from the PSE approach (N_f (PSE)), N_f from the DE approach (N_f (DE)), and Superpave fatigue parameter (|G*|.sinδ). The power law regression was found to be the best-fitted model for all

the combinations. Figure 5.4 to 5.7 presents the correlation between N_f (TS) and the other three variables for both geometries and binders.

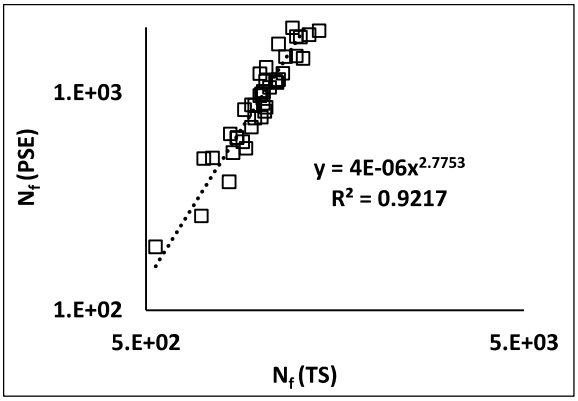

(a)

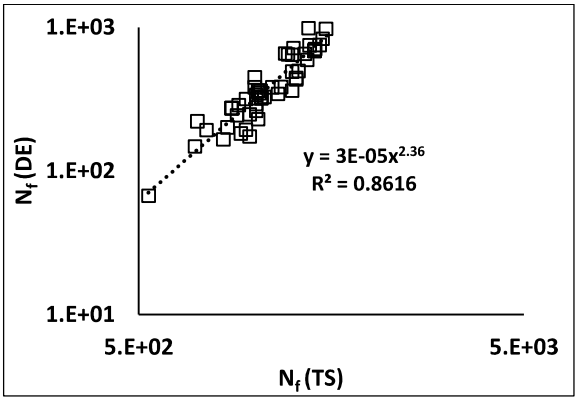

(b)

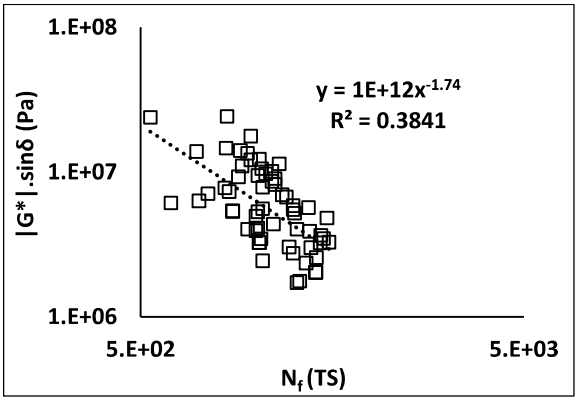

(c)

Figure 5.4 Correlation between N_f (TS) and (a) N_f (PSE), (b) N_f (DE), (c) $|G^*|.\sin\delta$ for hyperbolic geometry using VG-30 binder

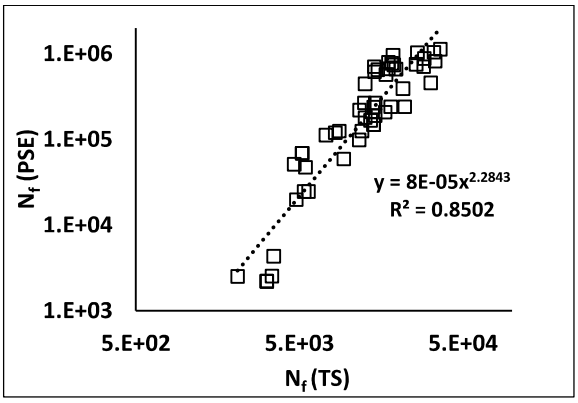

(a)

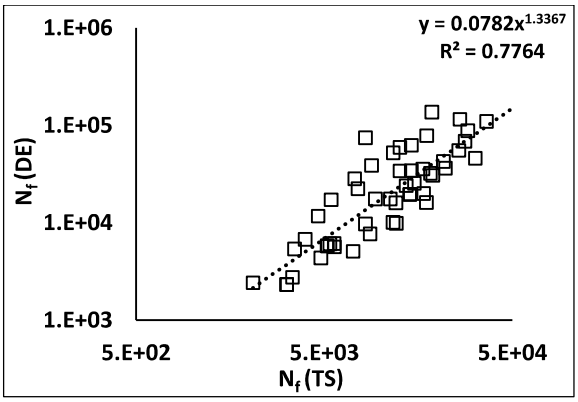

(b)

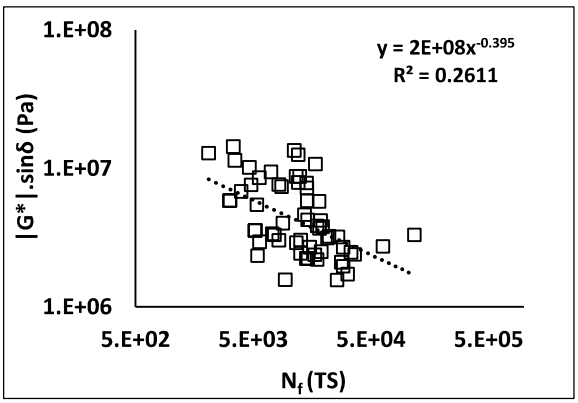

(c)

Figure 5.5 Correlation between N_f (TS) and (a) N_f (PSE), (b) N_f (DE), (c) |G*|.sinδ for hyperbolic geometry using PMB-40 binder

It is observed that the correlation between the TS test and LAS test using the PSE approach was found to be strongest, followed by DE and |G*|.sinδ. This observation was true irrespective of the binder and the testing geometry, which implied that the PSE approach was better than the DE approach in fulfilling the objectives. Previous studies have also reported the supremacy of PSE over DE [316]. In addition, the fatigue parameter and time sweep test have an extremely poor dependency with R^2<0.4 and hence |G*|.sinδ cannot be used as a TS alternative.

Moreover, the coefficient of determination (R^2) was higher with virgin binder as compared to the PMB, irrespective of other variables. The correlation between TS and (N_f (PSE)) was excellent in hyperbolic geometry, i.e., R^2=0.92 in VG and R^2=0.85 in PMB. On the other hand, the correlation was also quite strong, with R^2=0.75 in VG and R^2=0.71 in PMB in cylindrical geometry, but it was lower than that in HG. Therefore, the correlation analysis clearly showed that the LAS test may be considered as alternative to TS test using both the geometries but preferably, the HG is recommended for better simulation based on the binders considered in the present study.

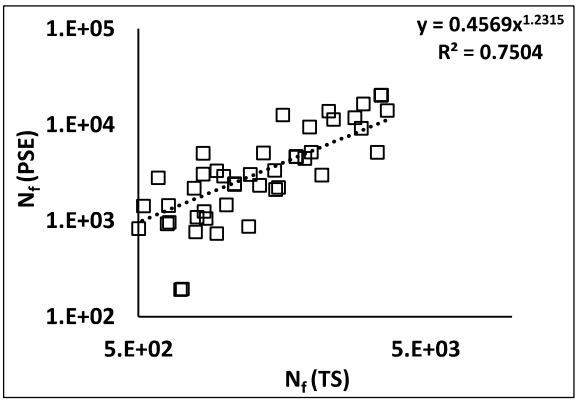

(a)

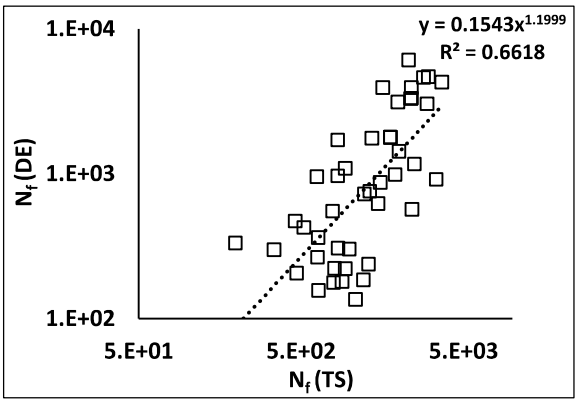

(b)

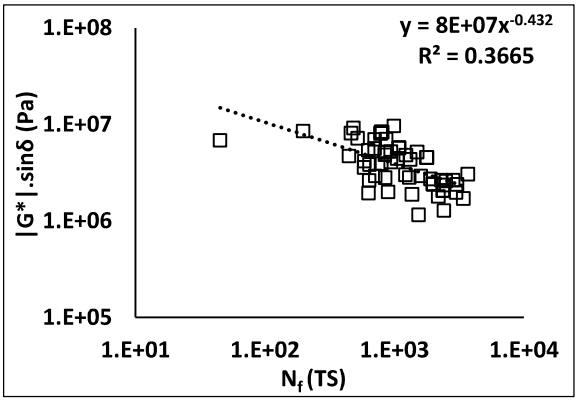

(c)

Figure 5.6 Correlation between N_f (TS) and (a) N_f (PSE), (b) N_f (DE), (c) $|G^*|.\sin\delta$ for cylindrical geometry using VG-30 binder

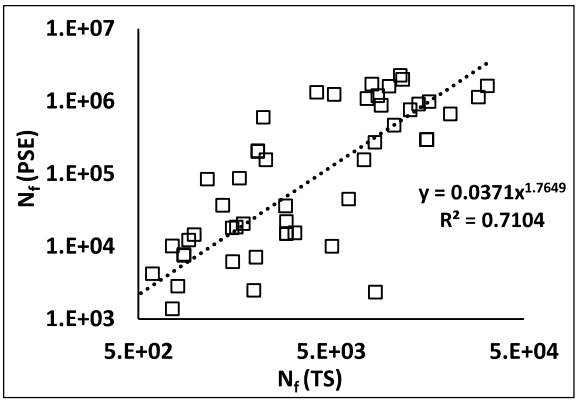
1.E+07
1.E+06
1.E+05
1.E+04
1.E+03
N_f (PSE)
y = 0.0371x^1.7649
R² = 0.7104
5.E+02
5.E+03
5.E+04
N_f (TS)

(a)

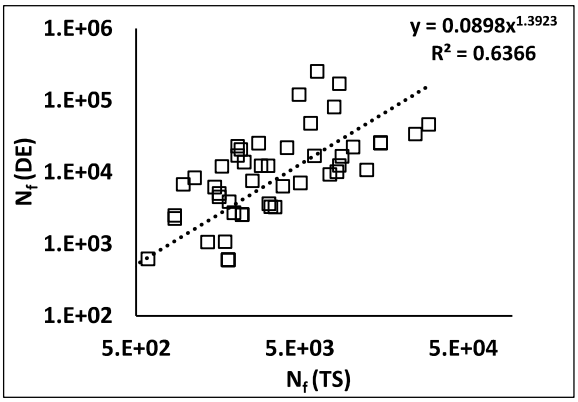
1.E+06
1.E+05
1.E+04
1.E+03
1.E+02
N_f (DE)
y = 0.0898x^1.3923
R² = 0.6366
5.E+02
5.E+03
5.E+04
N_f (TS)

(b)

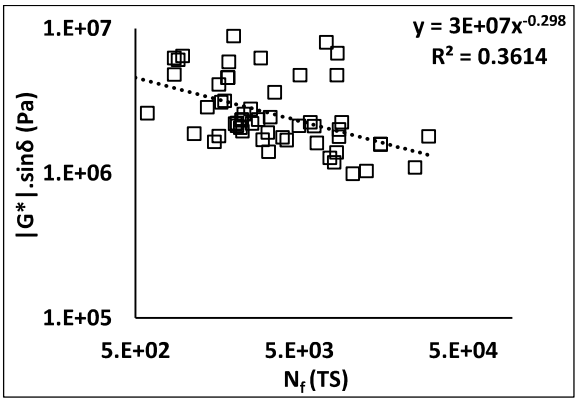
1.E+07
1.E+06
1.E+05
|G*|.sinδ (Pa)
y = 3E+07x^-0.298
R² = 0.3614
5.E+02
5.E+03
5.E+04
N_f (TS)

(c)

Figure 5.7 Correlation between N_f (TS) and (a) N_f (PSE), (b) N_f (DE), (c) $|G^*|.\sin\delta$ for cylindrical geometry using PMB-40 binder

5.5.2 Ranking Analysis

In addition to correlation analysis, the ranking analysis was also attempted to check whether the LAS test using the PSE approach could rank the materials in the same manner as the TS test. The LAS test cannot be adopted solely based on correlation analysis because it may be possible that the correlation between the TS and LAS test is good, but both tests rank the materials differently. This will be redundant because of the incompetency of the surrogate test to distinguish the materials in terms of their fatigue performance, similar to that of the TS test. A simple ranking analysis procedure was followed, assigning a higher numeral to the material having better performance. For example, rank 4 was considered better than rank 2 in this study; hence higher fatigue life was assigned a higher rank whereas a lower value of $|G^*|.\sin\delta$ corresponds to the better rank. This facilitates the uniform comparison among the various parameters. Table 5.1 Ranking analysis compares neat binder and different filler mastics at 10% filler concentration and 5°C temperature using hyperbolic geometry. The hypothesis was that the variable ((N_f (PSE)), (N_f (DE)), and ($|G^*|.\sin\delta$), which gives a ranking closer to the TS test, can be the potential candidate for the replacement because of the better simulation of the test results.

It is visible that the ranking of the materials was very similar to each other in the TS test and the LAS test using the PSE approach, whereas it was considerably different by using DE approach and fatigue parameter. Similar results were observed at all combinations of temperatures and filler-binder ratios for both types of binders, but only a single scenario is shown here for brevity. The ranking analysis complemented the results of the correlation

analysis and proved that the LAS test with the PSE approach of fatigue failure was able to rank the material in an exactly similar manner as the TS test.

The ranking analysis involved comparing the ranking of six fillers and one binder obtained from four different variables (TS, DE, PSE, and |G*|.sinδ) at different combinations of filler contents and testing temperatures due to which it may be difficult for the readers to compare the ranking corresponding to each test. Hence, an alternate method of data presentation was employed called discrepancy analysis to show the variation in the rankings.

Table 5.1 Ranking analysis

	Fatigue testing parameter			
Filler	**TS**	**PSE**	**DE**	**|G*|.sinδ**
Binder	3	3	5	7
RM	1	1	1	1
MD	7	7	7	3
LS	6	6	3	2
GR	4	5	4	6
BA	5	4	2	5
QZ	2	2	6	4

5.5.3 Discrepancy Analysis

In this study, ((N_f (TS)) is the reference variable, whereas the other three variables are ((N_f (PSE)), (N_f (DE)), and (|G*|.sinδ). The discrepancy analysis was used to better understand or quantify the comparison among the ranking of different variables. It consists of plotting the variables to be compared along the line of equality which is at a 45° angle from both axes. The discrepancy between the variables was assessed by the deviation of the data points (rank) from the equality line. Since there are six mastics and one base binder, a total of 7 data points were

plotted. The higher the number of points on the line of equality or nearer to that, the lower will be the discrepancy, and more will be the reliability.

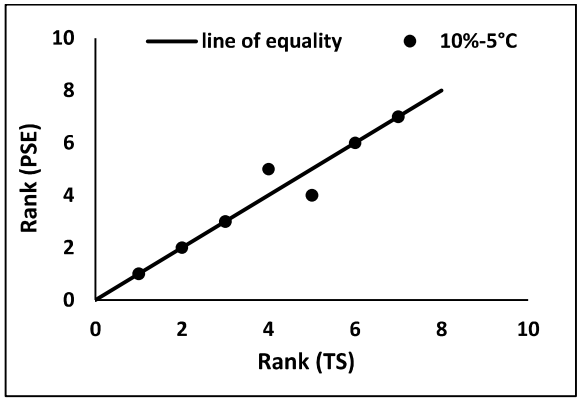

(a)

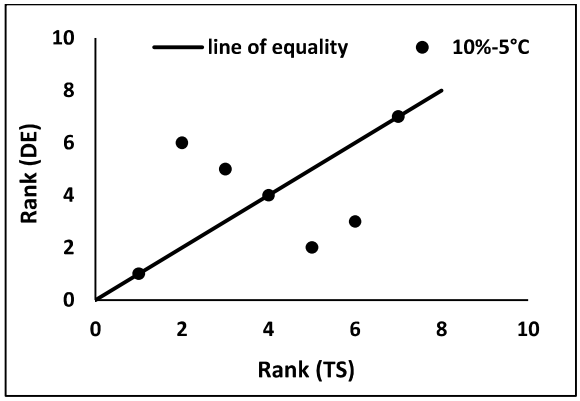

(b)

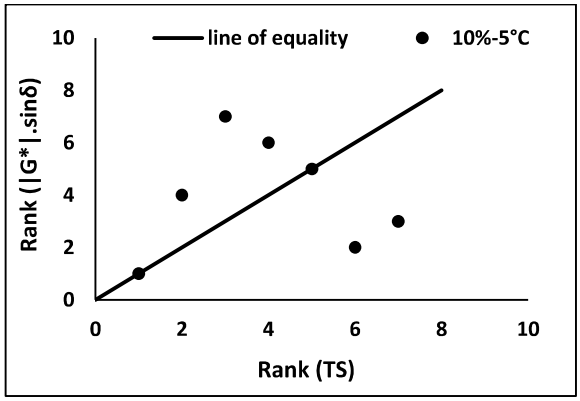

(c)

Figure 5.8 Discrepancy analysis between TS and (a) PSE (b) DE (c) $|G^*|.\sin\delta$ for hyperbolic geometry with VG-30 as the base binder

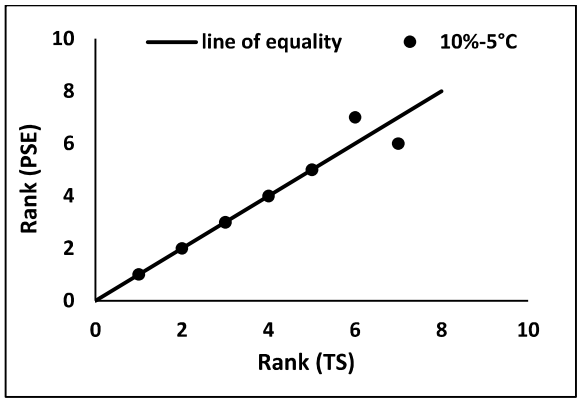

(a)

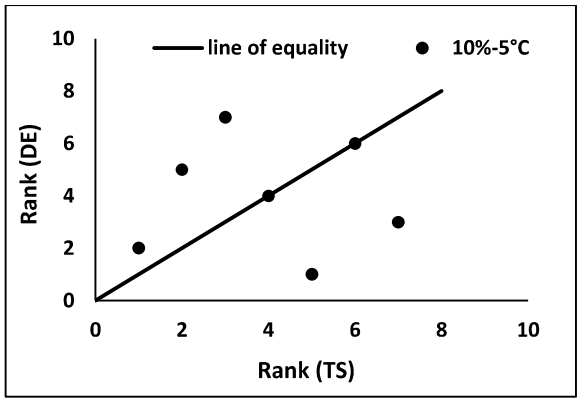

(b)

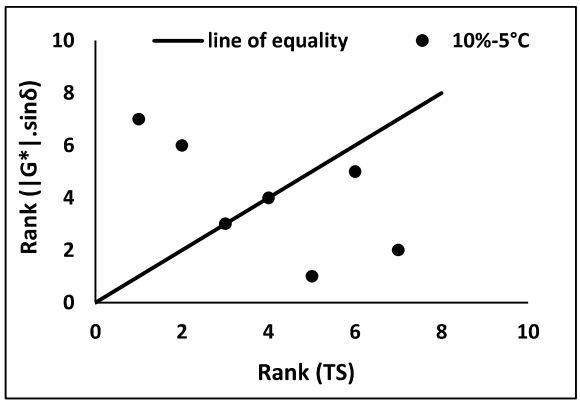

(c)

Figure 5.9 Discrepancy analysis between TS and (a) PSE (b) DE (c) |G*|.sinδ for hyperbolic geometry with PMB-40 as the base binder

Figure 5.8 and 5.9 present the discrepancy analysis at 10% filler content and 5°C temperature in the case of unmodified and polymer modified mastics, respectively, tested using hyperbolic geometry. The ranking obtained from the PSE approach was found to have the least deviation from the line of equality, followed by the DE approach and Superpave fatigue parameter. This observation was true for all the temperature and filler content combinations in both neat and polymer modified binders.

The lowest discrepancy between N_f (TS) and N_f (PSE) was also observed in most of the cases with cylindrical geometry for both VG and PMB but was relatively higher than HG (refer to Figure 5.10 and 5.11). In addition, inconsistencies were also observed in some cases where the lowest and highest discrepancy were difficult to distinguish due to the absence of a definite pattern, as shown in Figure 5.10.

The above results showed that the discrepancy analysis can provide a useful way of differentiating among the various mastics and help in finding the fatigue test, which simulates the time sweep test to a better extent. The strong correlation and lower discrepancy between the TS test and LAS test proved that the LAS can be used as the surrogate fatigue test in place of the TS test especially using the PSE approach.

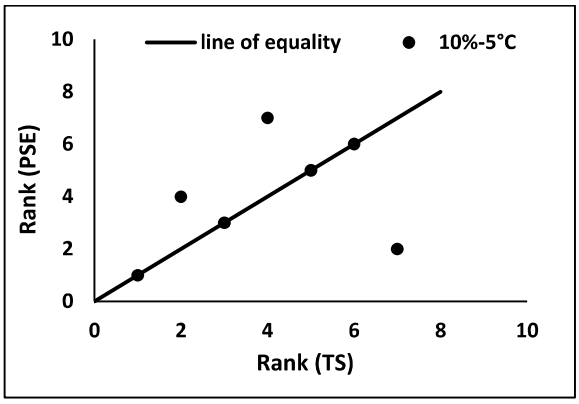
line of equality
10%-5°C
Rank (PSE)
Rank (TS)
0
2
4
6
8
10

(a)

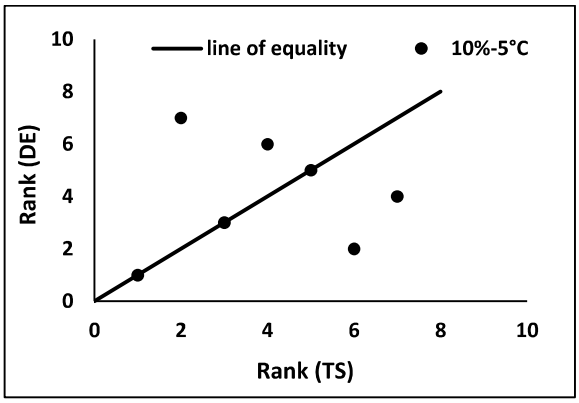
line of equality
10%-5°C
Rank (DE)
Rank (TS)
0
2
4
6
8
10

(b)

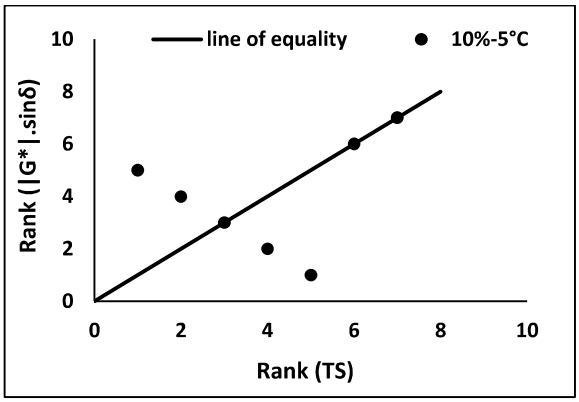
line of equality
10%-5°C
Rank (|G*|.sinδ)
Rank (TS)
0
2
4
6
8
10

(c)

Figure 5.10 Discrepancy analysis between TS and (a) PSE (b) DE (c) |G*|.sinδ for cylindrical geometry with VG-30 as the base binder

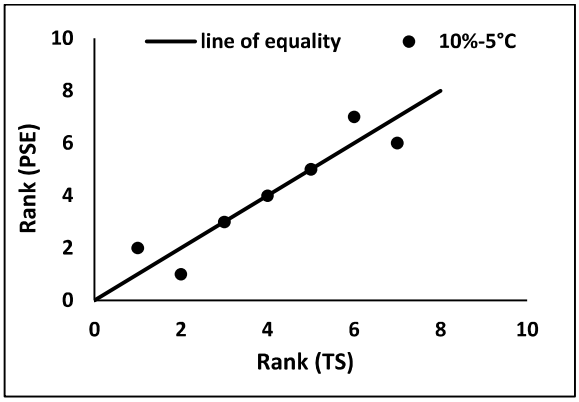

(a)

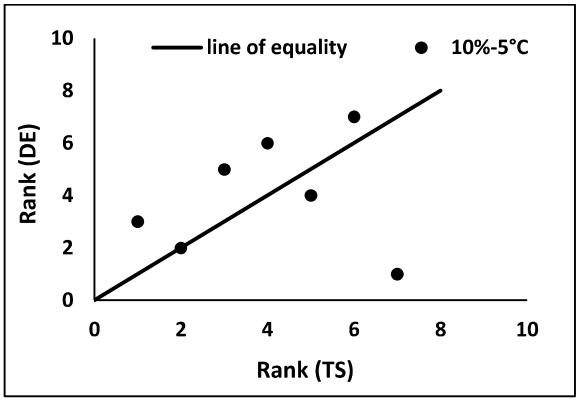

(b)

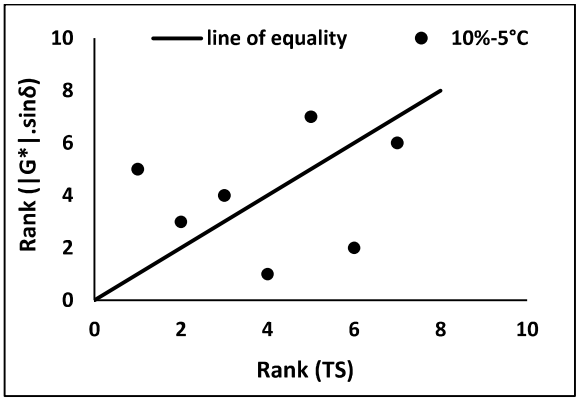

(c)

Figure 5.11 Discrepancy analysis between TS and (a) PSE (b) DE (c) |G*|.sinδ for cylindrical geometry with PMB-40 as the base binder

The drawbacks associated with the Superpave fatigue parameter, such as poor correlation with mixes and incapability to simulate higher damage, have already been discussed in section 2.4.4.1. Moreover, the DE approach hypothesized that all the energy is dissipated in the form of damage resulting from the applied load. But researchers have argued that some of the energy may get dissipated in the form of viscoelastic damping; hence, total DE cannot be due to damage alone [317]. Also, the loss of material integrity has been quantified using the phase angle in the DE approach, which again can't be solely due to damage but other parameters like nonlinearity, waveform distortion, and internal heating may also contribute [107]. Due to these reasons, the Superpave fatigue parameter and the DE-based approach used in the LAS test may not be able to exactly simulate the TS test. On the other hand, the peak stored PSE is considered as the failure point within the tested specimen in the PSE-based approach, and the effect of viscous damping has been eliminated from the total DE by replacing the pseudo strain in place of physical strain [317]. Hence, the actual damage is considered, due to which a strong correlation and the lowest discrepancy have been observed between the results of the TS test and LAS test using PSE based approach.

5.6 Efficacy of Hyperbolic Geometry as a Better Alternative to Cylindrical Geometry

The second objective of this chapter is to decide the better geometry for the accurate fatigue characterization of asphalt materials. The cylindrical geometry has been used in the DSR for a very long period of time, but the problems associated with it have been highlighted by several scholarly articles from time to time. The previous works of literature have strongly criticized

the novelty of using cylindrical PP geometry for the rheological analysis of asphalt materials due to the several lacunas, as discussed below.

When the asphalt material in the form of the cylindrical specimen is subjected to the loading, the damage starts at the edge or outer periphery of the material and advances towards the center with increasing loading cycles resulting in the reduced radius of the sample with increasing damage [40]. Therefore, the damage is non-uniform in the cylindrical sample, with the outer edge being fractured, but the center remains intact, as evident from specialized imaging techniques too [318,319] which may result in the underestimation of fatigue life. In addition, the stress distribution across the radius of the specimen is also non-uniform, as shown in Figure 5.12, due to which the accuracy of the complex modulus is questionable [40]. The shear stress is lowest at the center and increases with the distance from the center; hence the obtained modulus is not explicit, which may produce ambiguous results.

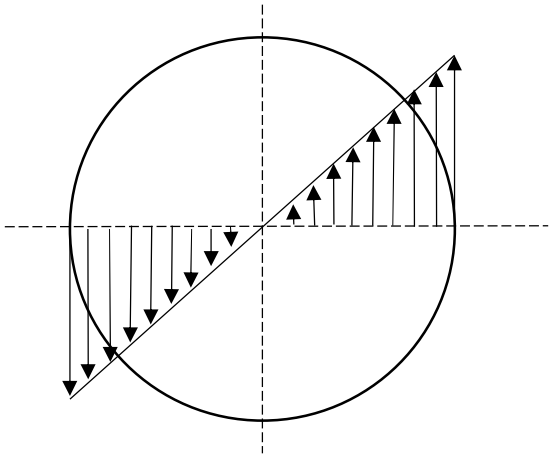

Figure 5.12 Shear stress variation in the cylindrical geometry [40]

The modified binder with a modifier of size more than 250 μm cannot be tested in the PP geometry, especially at high temperatures, since the gap size requirement is more than four times the maximum size of the particle as per AASHTO T 315 [42]. This problem has been rectified using alternate geometry, such as bob and cup geometry.

The cylindrical specimen of the asphalt sometimes fails earlier than the true fatigue failure when the complex modulus is relatively small (2-5 MPa), commonly known as edge instability or edge effect [197]. The edge effect is the loss of geometry at the boundary of the sample with the formation of indentation of the free surface of the liquid [320]. Due to the very low stiffness, the material is not able to hold itself at the edges, and flow-like indentation is observed. The cylindrical geometry is also very susceptible to interfacial/adhesion failure, especially for stiffer materials like asphalt mastics which are 3-6 times stiffer than neat binder (up to 11 times stiffer in this study). When the torque is applied to the excessively stiffer samples, the spindle slips from the surface of the specimen due to lack of adhesion; as a result, the applied torque is not transferred to the sample. Hence, a true cohesion failure is not obtained [17]. Hence, obtaining the true cohesive failure within the cylindrical specimen in PP geometry is a very big challenge itself.

The aforementioned lacunas clearly signify that the results of cylindrical geometry show discrepancy, especially with stiffer materials like asphalt mastics, and hence cannot be trusted.

Hence, an alternative geometry with better efficacy can be used to accurately characterize asphalt materials. Therefore, the current study is focused on assessing the suitability of hyperbolic geometry for the fatigue analysis of asphalt binders as well as asphalt mastics.

The conventional geometry cannot be discarded just by referring to the previous studies because of the different materials and testing conditions. Therefore, rather than directly using the alternate geometry, comprehensive testing was done on both geometries to check the discrepancies in the results obtained by cylindrical geometry.

Figure 5.13 shows the variation in fatigue life of asphalt mastic samples using the hyperbolic and cylindrical test geometry. The data is presented for red mud filler based mastics at different F-B ratios (10, 20, and 30%) and 5°C temperature for both binders. The first letter in the legend

stands for the type of analysis procedure (P-PSE based approach, D- DE based approach), and the second letter indicates the type of filler (R- red mud). The results at 5% strain for VG based mastics using hyperbolic geometry in the form of bar charts are also shown as an example in Figure 5.14 for better clarity.

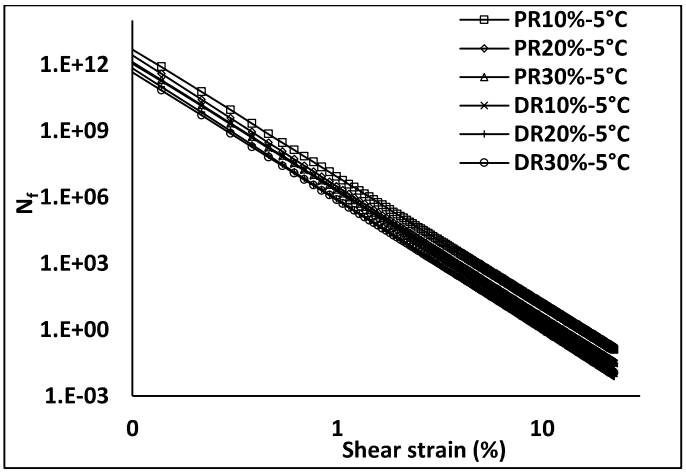

(a)

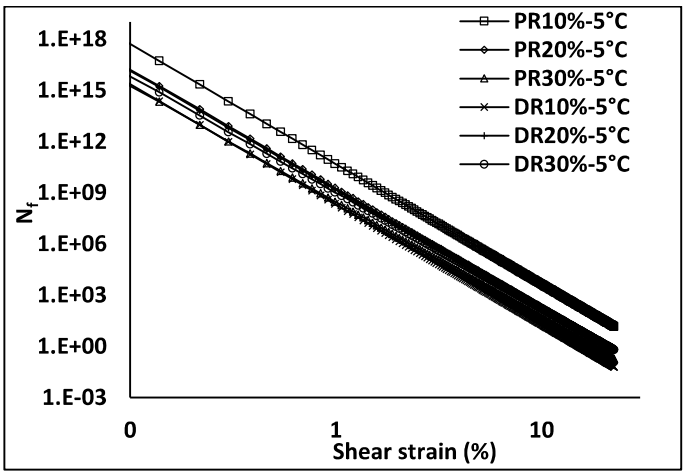

(b)

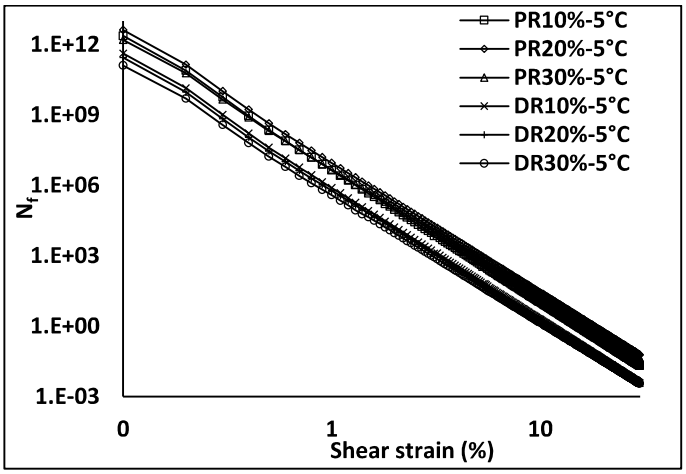

(c)

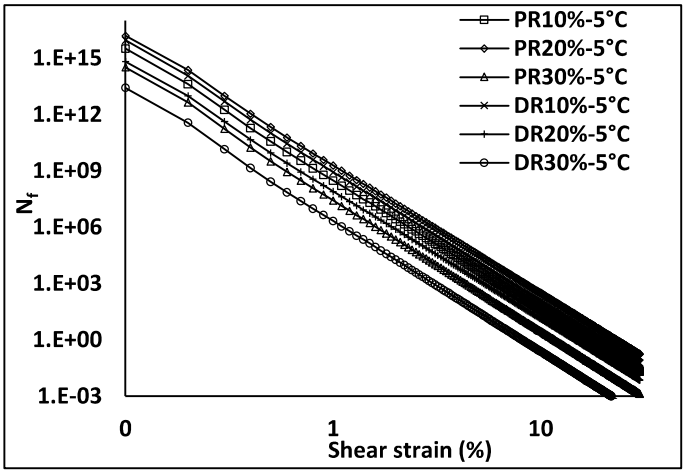

(d)

Figure 5.13 Comparative analysis between both fatigue analysis procedures for red mud filler at 5°C temperature for hyperbolic geometry using (a) unmodified binder (b) polymer modified binder and for cylindrical geometry using (c) unmodified binder (d) polymer modified binder

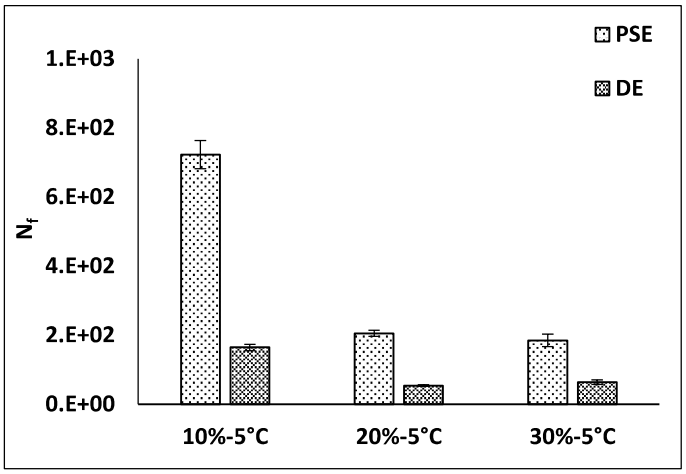

Figure 5.14 Comparison between the fatigue life at 5% strain obtained from both fatigue analysis procedures for red mud filler at 5°C temperature in case of hyperbolic geometry using VG-30 binder

It is observed that the PSE based approach yields a higher fatigue life as compared to the DE based approach. This observation is true for all possible combinations of the different variables used in the study, all of which are not shown for brevity. The current analysis is focused on selecting a reliable geometry by comparing the stiffening behavior of fillers at different filler contents. It is to be noted that this chapter discusses the feasibility of geometry based on relative stiffening only but not from the fatigue point of view. This is a generalized discussion and is not based on the particular type of distress; hence only the effect of fillers is considered. The increment or decrement of no. of cycles to failure or fatigue life of the specimen cannot be anticipated based on the filler content. The addition of filler may enhance or aggravate the fatigue resistance of the binder depending on the various factors, which is a completely different discussion and is detailed in the next chapter.

The damage is proportional to $|G^*|.\sin\delta$ and C^* (pseudostiffness) in the DE based approach and PSE based approach, respectively, as described in equations (2.15) and (2.27). Since the PSE approach was found to be the best suited method to be used as a TS alternative, the variation

of C* was studied to assess the discrepancy among the geometries. Figures 5.15 and 5.16 showed the comparison between the geometries in terms of the evolution of pseudostiffness with the change in shear strain amplitude corresponding to different fillers for VG-30 and PMB-40 binders, respectively. The first letter in the legend represents the type of filler (R-RM, M-MD, L-LS, G-GR, B-BA, and Q-QZ), whereas the testing geometry is represented by the second letter (C-cylindrical, H-hyperbolic) followed by the filler content and the testing temperature.

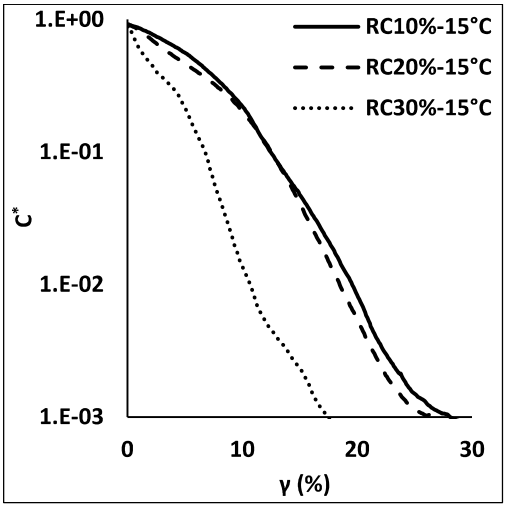

(a)

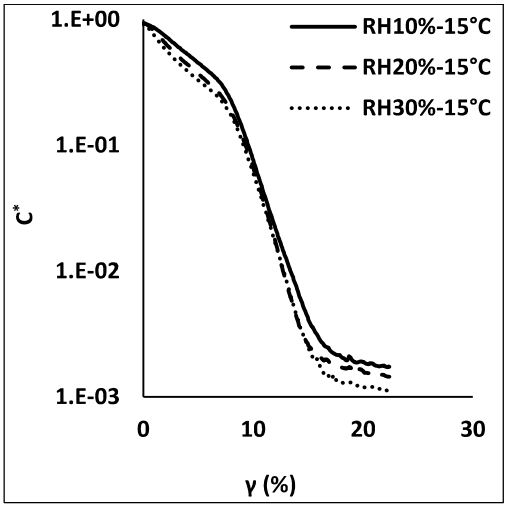

(b)

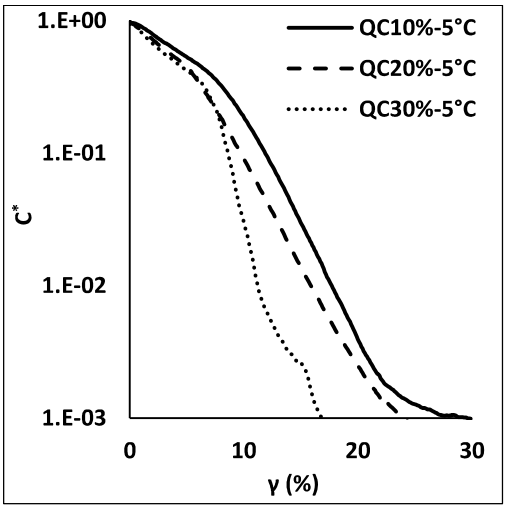

(c)

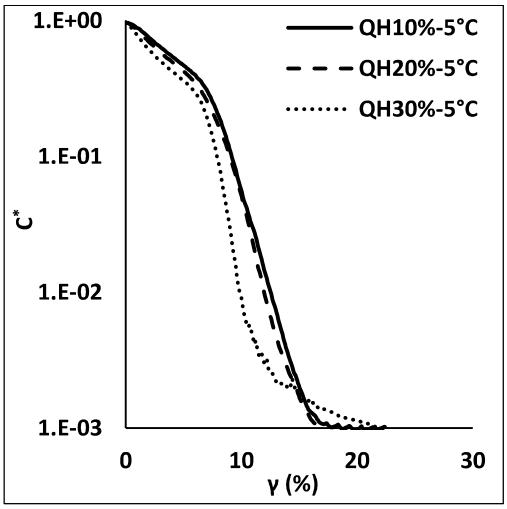

(d)

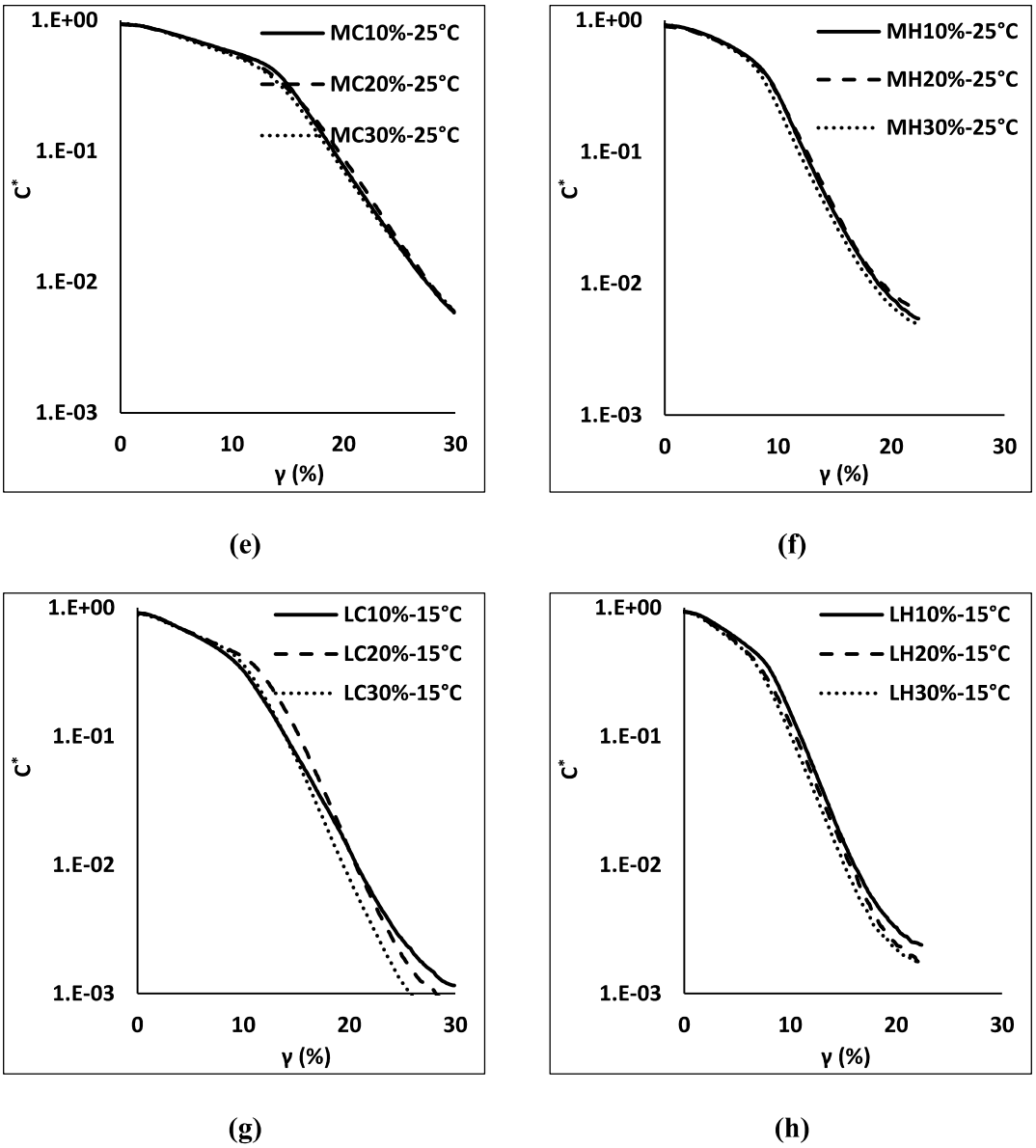

Figure 5.15 Comparison between the evolution of pseudostiffness with the change in shear strain in both the geometries at different fillers, temperatures, and filler-binder ratios in the case of unmodified mastics

It is clear from the comparative analysis between both the geometries that the behavior of materials is considerably different among geometries, notably at the highest filler content, i.e., 30%; hence both geometries cannot be accurate. One of the aforementioned geometry could be a better representative of the behavior of mastics as compared to the other. Therefore, a better

geometry should be chosen first to precisely represent the material behavior before going for further analysis.

Figure 5.15 shows that the value of C* consistently decreases with the increase in strain level, which signifies the damage. This induced damage in the asphalt materials as a result of increased loading is an inevitable phenomenon, but the damage rate influences the material's fatigue characteristics. A higher damage rate indicates sudden or brittle failure, whereas a smooth and steady rate shows gradual failure, although the ultimate failure cycles are dictated by the failure strain. It is observed that the rate of damage was smooth and gradual in the hyperbolic geometry with a definite pattern in the decrement of C^* irrespective of the type of filler, temperature, and the filler content. This shows that the material is failing from the defined failure location, and hence a definite cohesive failure is observed, and the accumulation of damage with the increase in strain is more precisely quantified. On the other hand, the damage rate was also quite similar in CG, but inconsistencies or abnormalities were observed in many cases, especially at higher filler content (30%). The damage rate was found to be significantly higher in such cases, as indicated by the sudden decrement in pseudostiffness. This may be attributed to the localized failure within the parallel plate, which induces a faster damage rate within the asphalt mastic. The excessively stiff asphalt material, when tested with cylindrical geometry, generally fails in adhesion [17]. The applied loading is not transferred to the sample before which a slippage occurs between the upper plate and the asphalt sample; hence the failure point obtained from the analysis is not the true failure. This sudden increase in the damage rate was not observed in every sample while testing with CG. For example, RM at 15°C and QZ at 5°C showed a sudden increase in the damage in cylindrical geometry, whereas MD at 25°C and LS at 15°C behaved similarly in both geometries.

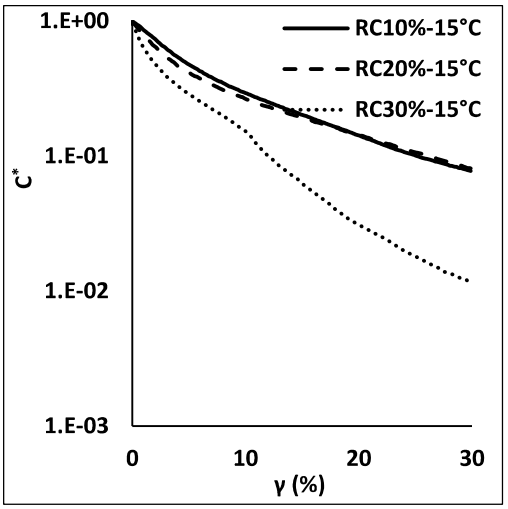
1.E+00
1.E-01
1.E-02
1.E-03
C*
0
10
20
30
γ (%)
RC10%-15°C
RC20%-15°C
RC30%-15°C

(a)

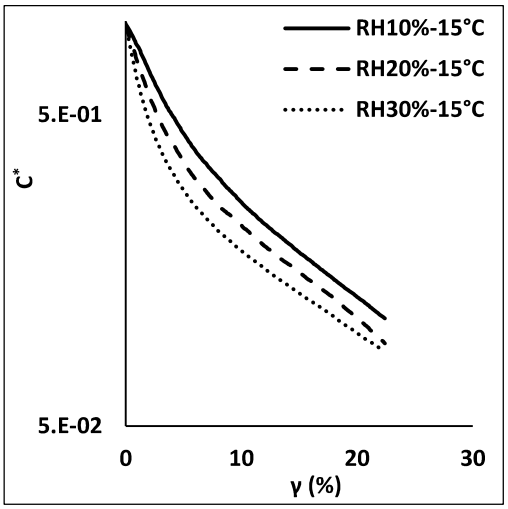
5.E-01
5.E-02
C*
0
10
20
30
γ (%)
RH10%-15°C
RH20%-15°C
RH30%-15°C

(b)

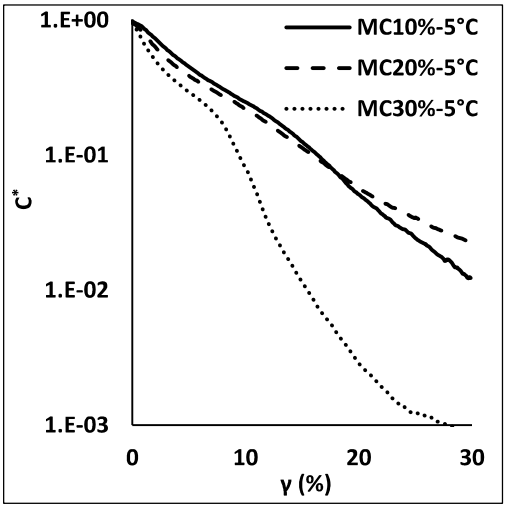
1.E+00
1.E-01
1.E-02
1.E-03
C*
0
10
20
30
γ (%)
MC10%-5°C
MC20%-5°C
MC30%-5°C

(c)

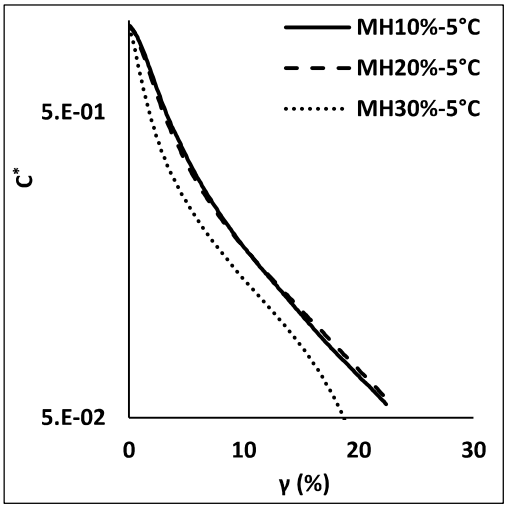
5.E-01
5.E-02
C*
0
10
20
30
γ (%)
MH10%-5°C
MH20%-5°C
MH30%-5°C

(d)

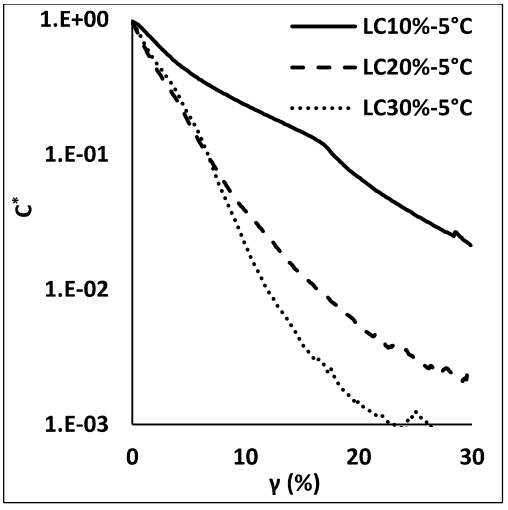
1.E+00
1.E-01
1.E-02
1.E-03
C*
0
10
20
30
γ (%)
LC10%-5°C
LC20%-5°C
LC30%-5°C

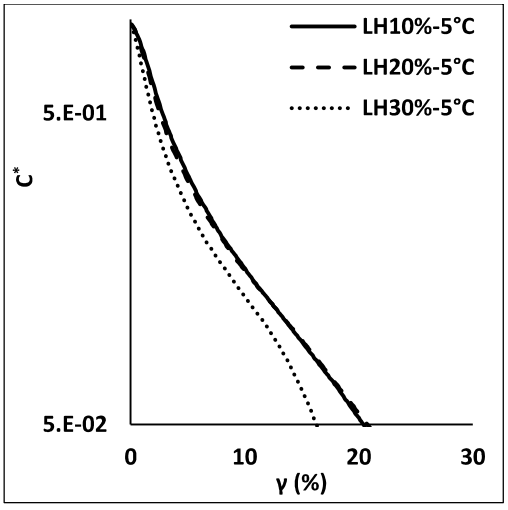
5.E-01
5.E-02
C*
0
10
20
30
γ (%)
LH10%-5°C
LH20%-5°C
LH30%-5°C

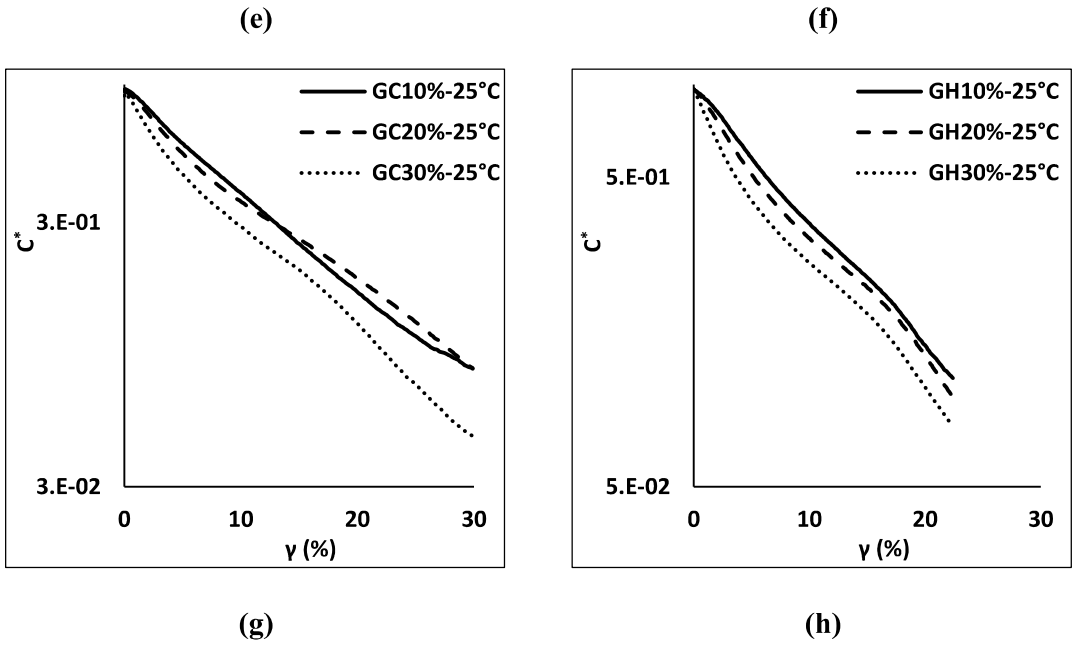

Figure 5.16 Comparison between the evolution of pseudostiffness with the change in shear strain in both the geometries at different fillers, temperatures, and filler-binder ratios in the case of polymer modified mastics

The aforementioned discussion was dedicated to the asphalt mastics prepared with VG-30 as the base binder. Figure 5.16 shows the variation in pseudostiffness as a function of applied shear loading in PMB based mastics. The ambiguity in the test results of CG was also reflected with polymer modified binder. The arbitrary change in the damage path was visible in different testing conditions, as evident from Figure 5.16 (a), (c), (e) similar to Figure 5.15 ((a) and (c) corresponding to RM and QZ respectively), whereas smooth transitions in the CG (Figure 5.16 (g)) were observed similar to Figure 5.15 ((e) and (g) corresponding to MD and LS respectively) in case of VG based mastics.

The results showed no definite pattern following which the sample will fail in adhesion. The excessive stiffness, which is mainly shown by 30% filler mastics, can be somehow attributed to such behavior, but there are many other factors involved, such as binder type, temperature, and type of filler with a wide range of physical properties due to which whether the sample

fails in true cohesion or not is uncertain. Hence, there are chances of discrepancies between the results obtained from the cylindrical geometry, as shown here, even if it cannot be concluded that the cylindrical geometry is erroneous.

5.7 Summary

The uncertainty in the testing time duration of a typical TS test demands a proxy test that can characterize the fatigue behavior of asphalt materials with similar efficiency and can be completed in a reasonable time duration. Also, the conventional cylindrical parallel plate geometry is often criticized due to the associated lacunas, and hence there is an immense need to explore the alternate geometry chosen as hyperbolic geometry in this study. It is a 3 mm high specimen geometry with a gradually decreasing diameter ranging from 8 mm to 6 mm from top/bottom to the center. The asphalt samples were evaluated using the TS and LAS tests on both geometries. The hyperbolic geometry testing results were multiplied by the respective conversion factors to account for the discrepancy in the results due to the software programming of the DSR corresponding to cylindrical geometry only.

The TS results were compared with the results of the LAS test using both DE and PSE approaches and the Superpave fatigue parameter using correlational analysis, ranking analysis, and discrepancy analysis. The LAS test was able to precisely quantify the behavior of the asphalt materials similarly to of TS test by using PSE based approach of fatigue failure. To investigate the efficacy of the alternate geometry, the LAS testing results obtained from both geometries were analyzed by studying the variation of pseudostiffness with the change in shear strain amplitude. The hyperbolic geometry was able to distinguish the relative stiffening caused by the addition of filler more accurately, whereas the inconsistencies in the form of arbitrary failure were observed in many cases with cylindrical geometry; hence the hyperbolic geometry was selected as the testing geometry for the further analysis in this study.